Schweizerischer Erdbebendienst
Service Sismologique Suisse
Servizio Sismico Svizzero
Servizi da Terratrembels Svizzer

ETH
Eidgenössische Technische Hochschule Zürich
Swiss Federal Institute of Technology Zurich

# Lucerne - Bramberg (SLUB)

## SITE CHARACTERIZATION REPORT

**Clotaire MICHEL, Valerio POGGI, Carlo CAUZZI**

**Jan BURJANEK, Daniel ROTEN, Donat FÄH**

Sonneggstrasse 5 CH-8092 Zürich Switzerland; E-mail: clotaire.michel@sed.ethz.ch

Last modified : November 5, 2013

# Abstract

Ambient vibration array measurements and active seismics following the MASW technique were performed on the molassic hill of Bramberg in the city of Lucerne. The site, where the new station SLUB of the Swiss Strong Motion Network was installed, is the reference station for the Lucerne basin (station SLUW). In order to characterize the velocity profile under the station, array measurements with a $160\,\mathrm{m}$ aperture and a $46\,\mathrm{m}$ long seismic line were performed. The combination of passive and active measurements was successful and allowed deriving a velocity model for this site. The soil column underlying station SLUB is made of a first layer of $10\,\mathrm{m}$ of a weak sandstone with an unclear velocity profile that is on average $700\,\mathrm{m/s}$. Below, a rock layer with velocities around $1500\,\mathrm{m/s}$ down to about $30\,\mathrm{m}$ depth is found at SLUB site. Hard rock is found at this depth with a velocity of $2700\,\mathrm{m/s}$. $V_{s,30}$ is found to be close to $1100\,\mathrm{m/s}$ corresponding to EC8 and SIA261 ground types A.

# Contents

# 1 Introduction

The station SLUB (Luzern Bramberg) is the rock reference station of the Swiss Strong Motion Network (SSMNet) for the Lucerne basin. SLUB has been newly installed in the framework of the SSMNet Renewal project in 2011. This project includes also the site characterization. In this project, passive array measurements have been selected as a standard tool to investigate these sites, but active seismics is also used especially for rock sites. A passive array measurement was therefore carried out on 15th May 2012 at this site (Fig. 1). In addition, in date 05.12.2011, an active seismic experiment has been performed, with the aim of mapping the phase velocity dispersion function of the surface-waves at high-frequency (>10Hz). The goal of the experiment is to extend the resolution of the passive seismic survey on the shallower part of the velocity model. The station is located on a molasse hill made of sandstone, within the city of Lucerne.

This report presents the measurement setup, the H/V analysis, the array analysis and the active seismic processing of the surface waves. The results of both measurements are compared and merged. Then, an inversion of these results for a velocity profile is performed. Standard parameters are derived to evaluate the amplification at this site.

| Canton | City | Location | Station code | Site type | Slope |
|---|---|---|---|---|---|
| Luzern | Lucerne | Bramberg | SLUB | Hill | Sloppy |

Table 1: Main characteristics of the study-site.

Figure 1: Picture of the site.

# 2 Experiment description

## 2.1 Ambient vibration sources

The ground surface is permanently subjected to ambient vibrations due to:

- natural sources (ocean and large-scale atmospheric phenomena) below $1\,\mathrm{Hz}$,
- local meteorological conditions (wind and rain) at frequencies around $1\,\mathrm{Hz}$ ,
- human activities (industrial machines, traffic…) at frequencies above $1\,\mathrm{Hz}$ [Bonnefoy-Claudet et al., 2006].

The objective of the measurements is to record these ambient vibrations and to use their propagation properties to infer the underground structure. First, the polarization of the recorded waves (H/V ratio) is used to derive the resonance frequencies of the soil column. Second, the arrival time delays at many different stations are used to derive the velocity of surface waves at different frequencies (dispersion).

## 2.2 Active seismic sources

For the active experiment, a special device was use as active source, consisting of mass of $120\,\mathrm{kg}$, dropped from a height of up to $2\,\mathrm{m}$ ($1.13\,\mathrm{m}$ used in this experiment) (see Fig. 2). Two shot-offset distances were tested ($18.5$ and $40\,\mathrm{m}$) because the distance at which the surface-waves start developing from the source is generally unknown (without some prior knowledge on the local velocity structure). Different consecutive wave-field excitations (6 to 12) have been performed for each source off-set, with the goal of improving the signal-to-noise ratio by stacking in the time (classical f-k method, [Lacoss et al., 1969]) or in the frequency (wavelet t-f-k method, [Poggi et al., 2012a]) domain.

## 2.3 Equipment

For the active seismic measurements, two types of instrumentation were used together (see Tab. 2 and Fig. 3); an array of 24 vertical geophones (10Hz corner frequency, GEODE system), with 2m distance between, and an array of 6 six-channel seismological stations, with 4m inter-distance. Combining these two equipments theoretically allows having the large spatial resolution (from the dense geophone array) together with the possibility of using three component recordings. Unfortunately, one of the seismological stations failed to record, reducing the number of usable acquisition points from 12 to 10 only. Each seismological station was equipped with two three-component velocity seismometers (Lennarz 3C, 5s eigenperiod) and a 24bit data-logger (Quanterra Q330) named NR02, NR04, NR06 and NR09. Each Quanterra datalogger can record on 2 ports namely A (channels EH1, EH2, EH3 for Z, N, E directions) and B (channels EH4, EH5, EH6 for Z, N, E directions). Synchronization between stations was assured by standard GPS. The sensors were placed on a metal tripod in a $20\,\mathrm{cm}$ deep hole for better coupling with the ground.

Figure 2: The 120kg dropping mass device which has been used as artificial source to stimulate the generation of Rayleigh waves.

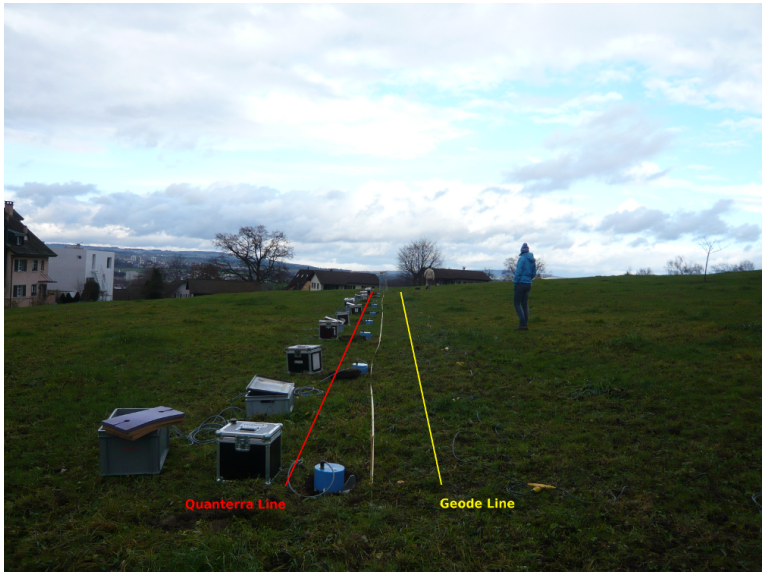


Figure 3: The two set of instruments used for the surface-wave survey. A geophone string of 24 elements (on the right) and 12 high-resolution three-component seismological stations (on the left).

For the passive measurements, 10 Quanterra Q330 dataloggers named NR01 to NR04 and NR06 to NR11 and 14 Lennartz 3C 5 s seismometers were used (see Tab. 2). Time synchronization was ensured by GPS. The sensor were placed on a metal tripod in a 20 cm deep hole, when possible, for better coupling with the ground.

| Experiment | Digitizer | Model | Number | Resolution |
|---|---|---|---|---|
| Active | | Geode | 10 | 24 bits |
| Active | | Quanterra Q330 | 6 | 24 bits |
| Passive | | Quanterra Q330 | 10 | 24 bits |
| **Experiment** | **Sensor type** | **Model** | **Number** | **Cut-off frequency** |
| Active | 1C Geophone | ? | 24 | 10 Hz |
| Active | Seismometer | Lennartz 3C | 12 | 0.2 Hz |
| Passive | Seismometer | Lennartz 3C | 14 | 0.2 Hz |

Table 2: Equipment used.

## 2.4 Geometry of the arrays

For the active seismic measurements, 2 parallel seismic lines of 24 geophones and 12 seismometers were installed, with a spacing of respectively 2 and 4 m, i.e. with a length of 46 and 44 m, respectively (Fig. 4).


Figure 4: Location of the seismic line (in red) and the two wave-field excitations (A at 18.5 m and B at ≈ 40 m) with green stars.

For the passive measurement, two array configurations were used, for a total of 4 rings of 10, 20, 40 and 80 m radius around a central station. The first configuration includes the 3 inner rings with 13 sensors (one point of the third ring could not be recorded because of a missing

cable); the second configuration includes the 2 outer rings with 11 sensors. The minimum inter-station distance and the aperture are therefore 10 and 80 m and 10 and 160 m, respectively. The experimental setup is displayed in Fig. 5. The final usable datasets are detailed in section 3.2.


Figure 5: Geometry of the arrays (blue triangles) compared to the seismic line (purple).

## 2.5 Positioning of the stations

The relative positioning of the sensors for the active experiment was performed using a measuring tape, with an accuracy of 10 cm. The absolute positioning of the seismic line was performed on the Swissimage, with an accuracy of 2 m.
The sensor coordinates of the array were measured using a differential GPS device (Leica Viva), including only a rover station and using the Real Time Kinematic technique provided by Swisstopo. It allows an absolute positioning with an accuracy of about 3 cm on the Swissgrid. For, some of the points below trees, this accuracy was not reached due to reflections of the GPS signal but it was always better than 6 cm.

# 3 Data quality

## 3.1 Usable data

From the active experiment, for each wave-field excitation, a recording of about 2s was performed when using the GEODE data-logger. These consecutive recordings have been then merged in a unique continuous stream of data, removing the noisy tail of the traces (Fig. 6). Conversely, the seismological stations recorded continuously, so that a manual selection of the usable part of the recording had to be performed. Station NR05 failed and point LUB008 in the E direction shows strange features and should not be used. It has to be noticed that not all the shots were identically successful during the experiment. Therefore, a further selection on the quality of the wave-field excitation has been performed. As such, only the best shots were selected (see 7) and gathered into a continuous stream. Datasets 1 and 2 have an offset of $18.5\,\mathrm{m}$, datasets 3, 4, 5 and 6 an offset of $40\,\mathrm{m}$.

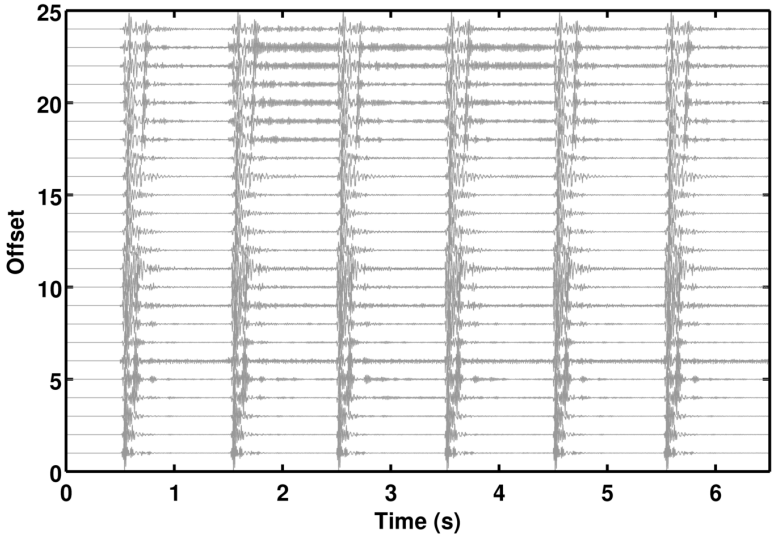


Figure 6: Example of six consecutive wave-field excitations using the 120kg dropping mass. Note that the time interval between consecutive shots has been artificially shortened, in order to remove the not-usable part of pure noise.

For the passive array, the largest time windows were extracted, for which all the sensors of the array were in position and the GPS synchronization was ensured. Strong wind ($20 - 40\,\mathrm{km/h}$) was blowing during the whole measurement. It affects the spectra below $0.8\,\mathrm{Hz}$ in Vertical but $2\,\mathrm{Hz}$ in the horizontal components. Component E of point LUB101 failed and the vertical components shows undamped peaks in the spectra due to interferences. A peak at $10\,\mathrm{Hz}$ is found in the N component of all recordings, it may be due to the tunnel below the hill. Large disturbances are present above $20\,\mathrm{Hz}$. Orientation of the sensors was checked by maximizing the correlation with the central station at low frequencies [Poggi et al., 2012c]. Deviations lower than $8\,^\circ$ were found for all points except point LUB301 ($16\,^\circ$). Original and rotated datasets are available for the 3C array analysis even though non-rotated was used here.

The characteristics of the datasets are detailed in Tab. 3.

## 3.2 Data processing

The data from the Quanterra stations were first converted to SAC format, including in the header the sensor coordinates (CH1903 system), the recording component and a name related to the position of the station. The name is made of 3 letters characterizing the location (LUB here) and 3 digits. For the active line, numbers are increasing from 001 to 012, for the passive array, 1 digit stands for the ring and 2 more digits for the number in the ring. Recordings were not corrected from the instrumental response.

| **Dataset** | **Starting Date** | **Time** | **Length** | $F_s$ | **Min. inter-distance** | **Aperture** | **# of points** |
|---|---|---|---|---|---|---|---|
| active | 2011/12/05 | 12:27 | 130 min | 200 Hz | 4 m | 44 m | 10 |
| 1 | 2012/05/15 | 10:15 | 98 min | 200 Hz | 10 m | 80 m | 13 |
| 2 | 2012/05/15 | 12:25 | 115 min | 200 Hz | 10 m | 160 m | 11 |

Table 3: Usable datasets from the seismological stations.

# 4 H/V processing

## 4.1 Processing method and parameters

In order to process the H/V spectral ratios, several codes and methods were applied to the passive data. The classical H/V method was applied using the Geopsy `http://www.geopsy.org` software. In this method, the ratio of the smoothed Fourier Transform of selected time windows are averaged. Tukey windows (cosine taper of 5% width) of $50\,\mathrm{s}$ long overlapping by 50% were selected. Konno and Ohmachi [1998] smoothing procedure with b=60 was used. The classical H/V of Fäh et al. [2001] was also applied.

Moreover, the time-frequency analysis method [Fäh et al., 2009] was used to estimate the ellipticity function more accurately using the Matlab code of V. Poggi. In this method, the time-frequency analysis using the Wavelet transform is computed for each component. For each frequency, the maxima over time (10 per minute with at least $0.1\,\mathrm{s}$ between each) in the TFA are determined. The Horizontal to Vertical ratio of amplitudes for each maximum is then computed and statistical properties for each frequency are derived. A Cosine wavelet with parameter 9 was used. The mean of the distribution for each frequency is stored. For the sake of comparison, the time-frequency analysis of Fäh et al. [2001], based on the spectrogram, was also used, as well as the wavelet-based TFA coded in Geopsy.

The ellipticity was also extracted using the Capon analysis [Poggi and Fäh, 2010] (see section on 3C array analysis) and also plotted on Fig. 8.

| Method | Freq. band | Win. length | Anti-trig. | Overlap | Smoothing |
|---|---|---|---|---|---|
| Standard H/V Geopsy | $0.2-20\,\mathrm{Hz}$ | $50\,\mathrm{s}$ | No | 50% | K&O 60 |
| Standard H/V D. Fäh | $0.2-20\,\mathrm{Hz}$ | $30\,\mathrm{s}$ | No | 75% | - |
| H/V TFA Geopsy | $0.2-20\,\mathrm{Hz}$ | Morlet m=8 fi=1 | No | - | - |
| H/V TFA D. Fäh | $0.2-20\,\mathrm{Hz}$ | Specgram | No | - | - |
| H/V TFA V. Poggi | $0.2-20\,\mathrm{Hz}$ | Cosine wpar=9 | No | - | No |

Table 4: Methods and parameters used for the H/V processing.

## 4.2 Results

H/V curves are consistent for all the recordings for the active data except LUB008 as explained before that shows a strange behaviour (Fig. 7). Moreover, all the methods to compute H/V ratios are compared on Fig. 8, in which the classical methods were divided by $\sqrt{2}$ to account for Love waves contribution [Fäh et al., 2001]. The matching above the resonance frequency is good except smoothing issues. However, the peak at $0.6\,\mathrm{Hz}$ is most likely due to wind. The case of the peak at $1.2\,\mathrm{Hz}$ is not clear.

For the passive data, the results are the same except that the wind was stronger making the peak at $0.6\,\mathrm{Hz}$ stronger and very variable through the array. The frequencies of interest for this measurement are anyway above $3\,\mathrm{Hz}$. The comparison with the 3C FK analysis is successful, but considering the array size, this concerns only frequencies above $3.5\,\mathrm{Hz}$. It shows that the wind is not much affecting the frequencies of interest.

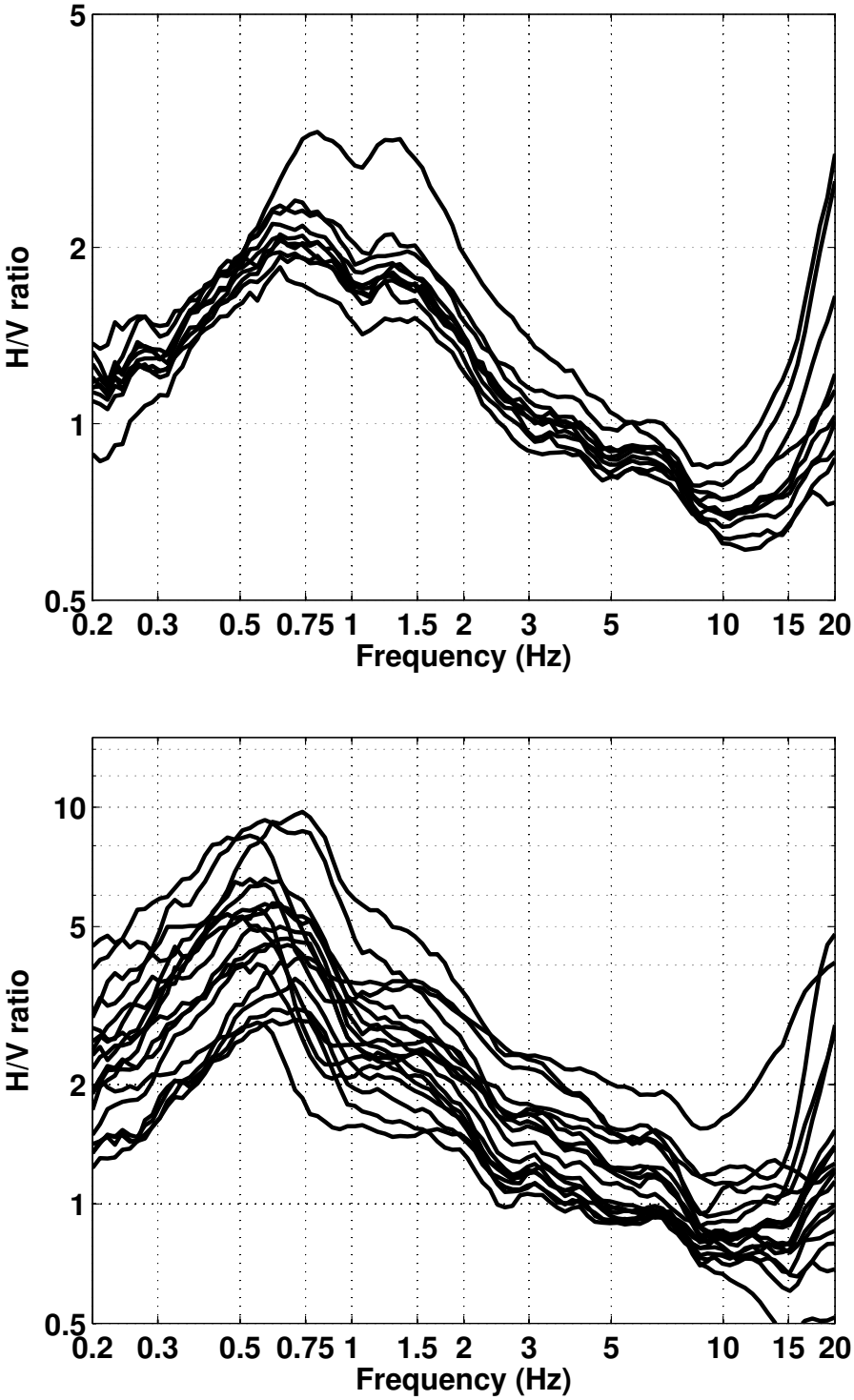


Figure 7: H/V spectral ratios (time-frequency analysis code V. Poggi) for the active (top) and the passive (bottom) experiments.

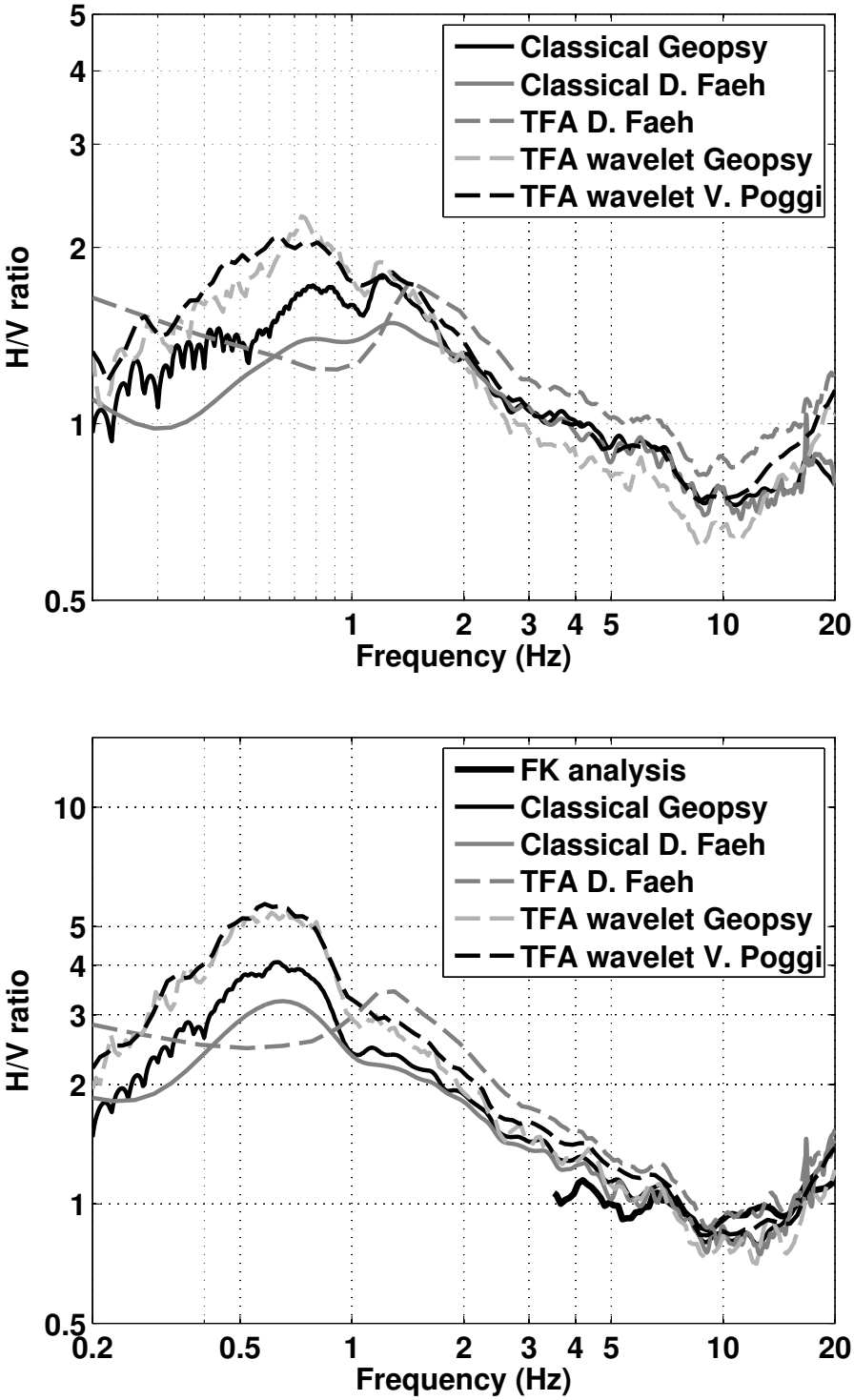


Figure 8: H/V spectral ratios for point LUB001 (active) and LUB000 (passive) using the different codes. Classical methods were divided by $\sqrt{2}$.

# 5 Processing

## 5.1 Processing methods and parameters of the active data

From the geophone recordings only the vertical direction is available for processing, while from the seismological stations both the vertical (channel 3) and the radial (channel 2) directions of recording have been analyzed. In all cases the classical f-k approach and the t-f-k analysis [Poggi et al., 2012a] have been used, providing nevertheless comparable results. In this report, then, only the results from the second method are presented. A tentative analysis of the transverse direction was also made, but the results have not been included in this report, since the employed sources do not give the possibility to directly generate anti-plane motion, and it is consequently not possible to rely on those results. Therefore, the following considerations are representative of Rayleigh-wave dispersion only.

## 5.2 Processing methods and parameters for the passive data

The vertical components of the arrays were processed using the High-resolution FK analysis [Capon, 1969] using the Geopsy `http://www.geopsy.org` software. Better results were obtained using large time windows (300T). The results in the FK plane were concatenated.

Moreover, a 3C array analysis [Fäh et al., 2008] was also performed using the Array Tool 3C software [Poggi and Fäh, 2010] using the Capon SVD method. It allows to derive Rayleigh and Love modes. The results of computations of both datasets were merged to estimate the dispersion curves.

| Method | Set | Freq. band | Win. length | Anti-trig. | Overlap | Grid step | Grid size | # max. |
|---|---|---|---|---|---|---|---|---|
| HRFK 1C | 1 | $2-40\,\mathrm{Hz}$ | $300T$ | No | 50% | 0.006 | 1.3 | 5 |
| HRFK 1C | 2 | $2-40\,\mathrm{Hz}$ | $300T$ | No | 50% | 0.002 | 1.3 | 5 |
| HRFK 3C | 1 | $2-30\,\mathrm{Hz}$ | $20T$ | No | 5% | 700 | 4500 | 5 |
| | | | Tap. 0.1 | | | m/s | m/s | |
| HRFK 3C | 2 | $2-30\,\mathrm{Hz}$ | $20T$ | No | 5% | 700 | 4500 | 5 |
| | | | Tap. 0.1 | | | m/s | m/s | |

Table 5: Methods and parameters used for the array processing.

## 5.3 Obtained dispersion curves from the passive analysis

For unknown reason, file LUB303 was corrupted and was removed from the 1C analysis. Both 1C and 3C (Fig. 9) analysis provided similar results. The Rayleigh fundamental mode could be picked between $5$ and $13.5\,\mathrm{Hz}$ including its standard deviation. Velocities range from $3000\,\mathrm{m/s}$ at $5\,\mathrm{Hz}$ down to $1800\,\mathrm{m/s}$ at $13.5\,\mathrm{Hz}$. The first higher mode can be picked from $15$ to $30\,\mathrm{Hz}$. The mode jumping at $14\,\mathrm{Hz}$ is not obvious from these results only, but it much clearer when passive and active dispersion curves are put together.

Moreover, the SVD method allowed to derive the ellipticity of the Rayleigh mode [Poggi and Fäh, 2010], with resolution down to 3.5 Hz.

The transverse component allows to pick the fundamental Love mode between 5 and 25 Hz including its standard deviation (Fig. 9). It is relatively similar to the Rayleigh mode.

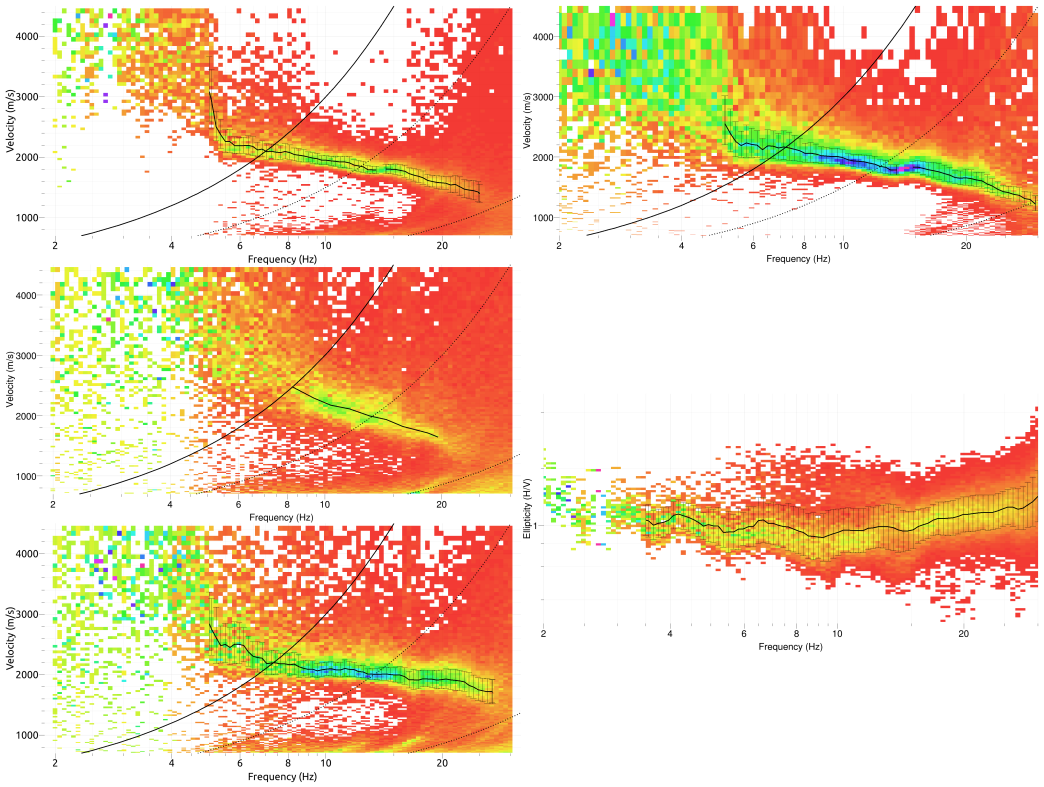


Figure 9: Dispersion curves obtained from the 3C array analysis (left): Top: Vertical - Centre: Radial - Bottom: Transverse component, and the 1C analysis (top right), as well as ellipticity from the 3C analysis (bottom right).

## 5.4 Obtained dispersion curves from the active analysis and merging with the passive results

The results using the two equipments are comparable for the vertical component of motion (Fig. 10). Two surface wave modes are clearly identifiable in the velocity-frequency plane. The fundamental mode is stable up to 30 Hz and extends nicely the estimate from passive recording of ambient vibration (Figure 5, green curve). At 30 Hz a large velocity jump is observable, where the fundamental mode drops from about 1200m/s to 600m/s. At the same frequency also the first higher mode starts to develop, and it can easily be tracked up to 80Hz.

Interpretation of the results from the processing of the radial direction is more difficult. In this case the fundamental mode has slightly higher velocities with respect to the vertical direction in the low frequency range (Fig. 11). In such a way, it doesn't match anymore the results from the passive seismics. Above 30Hz, both the fundamental and the higher modes cannot easily be tracked anymore. There might be several reasons for such discrepancy; as

first, anisotropy of the underground velocity structure can be present, which leads to different surface-wave propagation patterns in the vertical and the radial directions. On the other side, this can also be interpreted as an artifact of the processing, when the energy on the radial component is insufficient to produce an image of the dispersion. Unfortunately, we don't have any mean to propend for an interpretation or for the other at the present level of knowledge. Therefore, the results obtained from the radial component were not taken as granted.

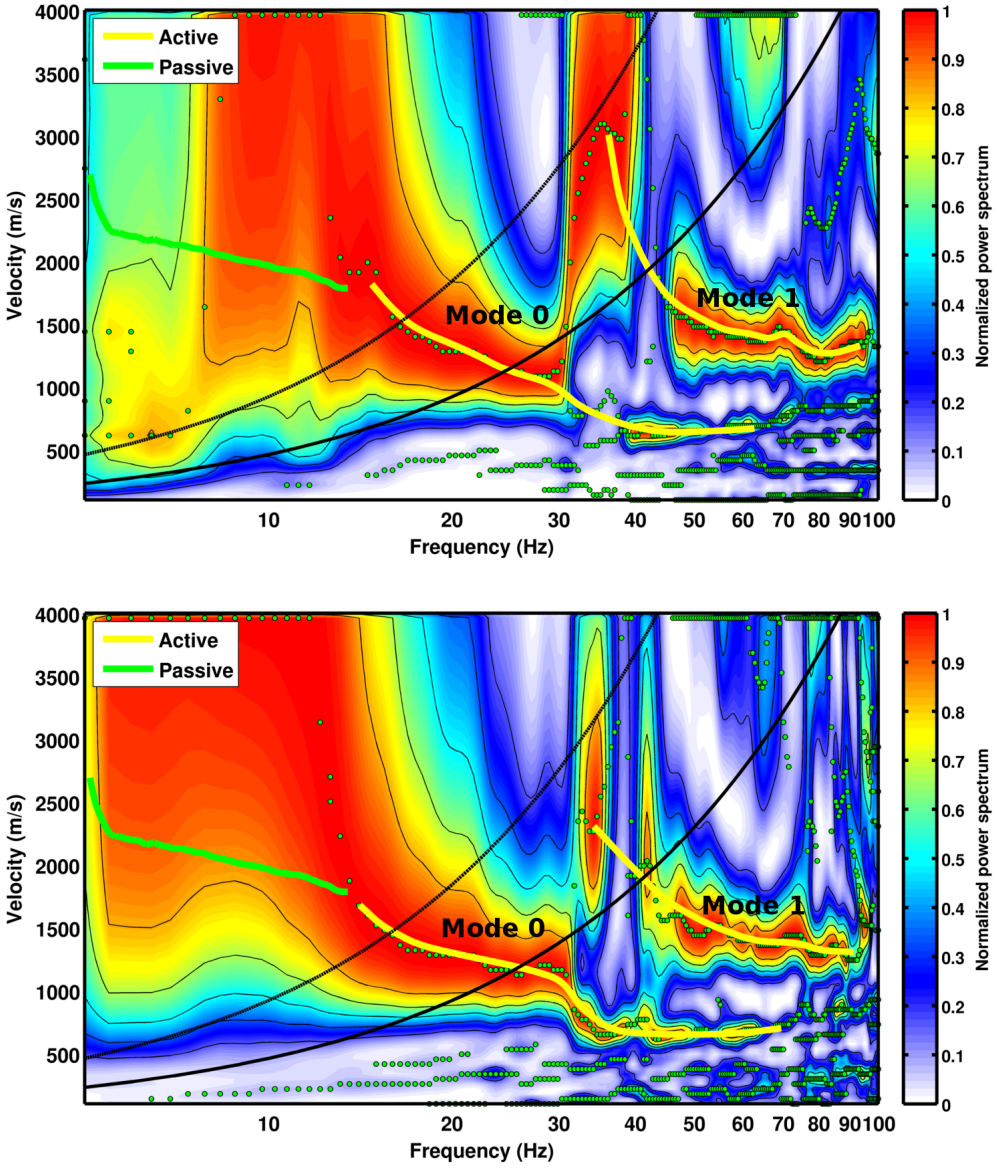


Figure 10: Results of processing the vertical direction using the geophone string (top) and the Lennartz sensors (bottom). In both cases, the analysis was performed with the wavelet t-f-k approach. In green, the portion of fundamental mode dispersion curve from passive acquisition of natural ambient vibration (array measurement).

Using Fig. 12, the extracted Rayleigh dispersion curves were finally interpreted as follows. The fundamental Rayleigh mode is the concatenation of the fundamental passive and active modes extracted from the vertical component Fig. 13. The first Rayleigh higher mode is found on the vertical component of the passive measurement as well as on the radial component of

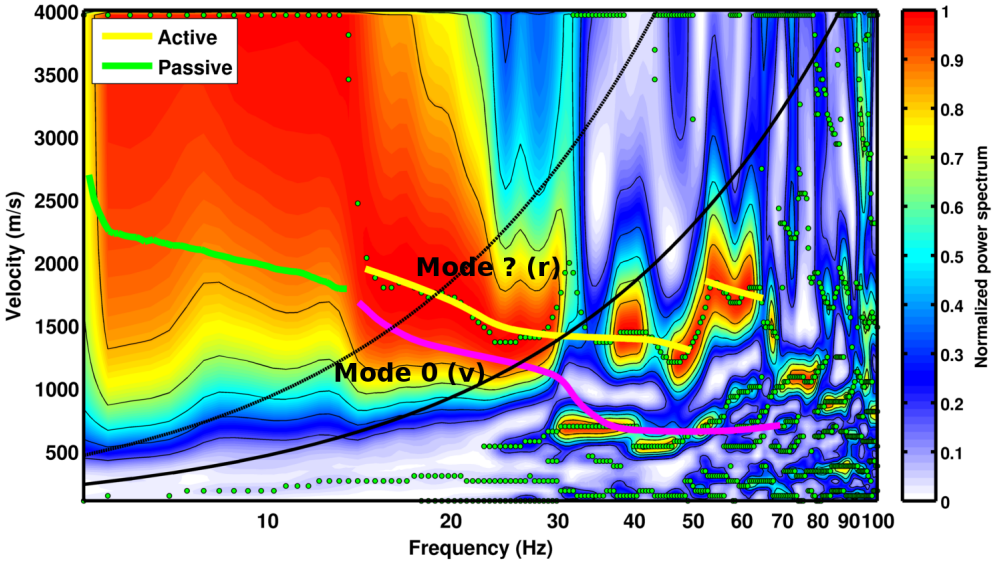


Figure 11: Results of processing the radial direction using the Lennartz sensor array. The picked fundamental mode is compared with the same one but from the vertical direction (Fig. 10)-bottom.

both active and passive data. What was previously thought to be the first higher Rayleigh mode from the vertical component of the active experiment is finally interpreted as the second higher mode.

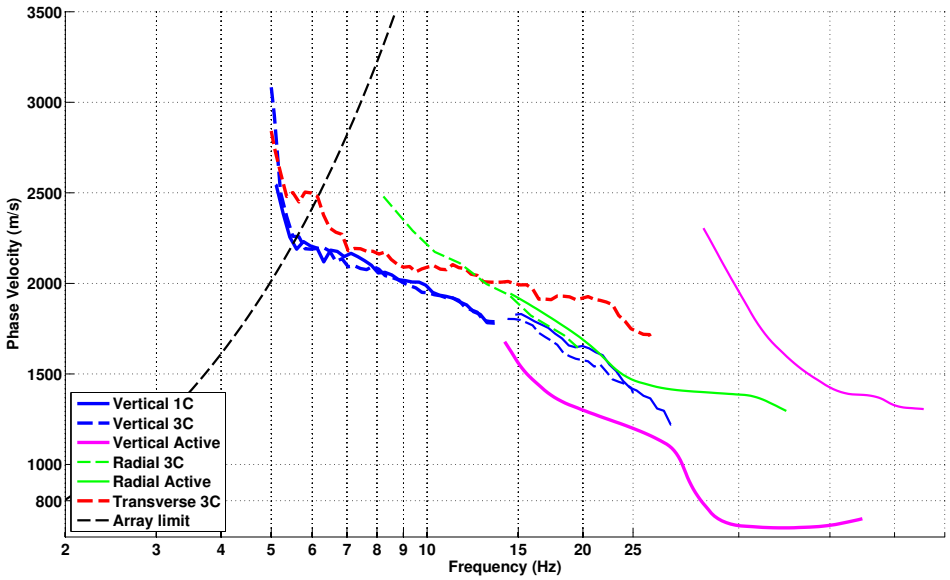


Figure 12: Picked dispersion curves from 1C and 3C analyses.

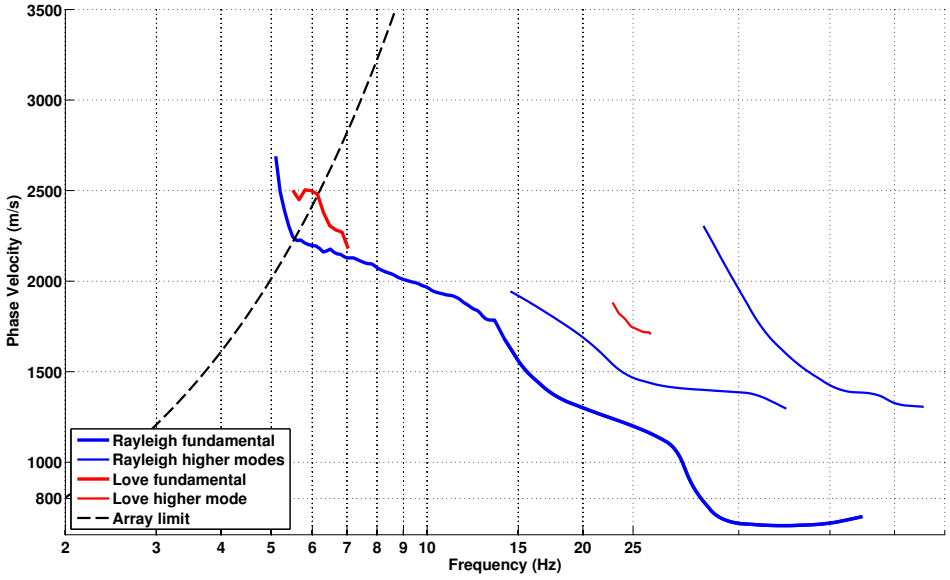


Figure 13: Interpreted dispersion curves selected for the inversion.

# 6 Inversion and interpretation

## 6.1 Inversion

For the inversion, only the Rayleigh modes were used. The fundamental mode ($5.6 - 70\,\mathrm{Hz}$) from the passive and the active measurement, the first ($15 - 50\,\mathrm{Hz}$) and the second ($35 - 90\,\mathrm{Hz}$) higher modes from the active measurement were used as simultaneous targets. All curves were resampled using 50 points between $5$ and $100\,\mathrm{Hz}$ in log scale. After tests with Love modes, they were re-interpreted as presented in Fig. 13.

The inversion was performed using the Improved Neighborhood Algorithm (NA) Wathelet [2008] implemented in the Dinver software. In this algorithm, the tuning parameters are the following: $Ns_0$ is the number of starting models, randomly distributed in the parameter space, $Nr$ is the the number of best cells considered around these $Ns_0$ models, $Ns$ is the number of new cells generated in the neighborhood of the $Nr$ cells ($Ns/Nr$ per cell) and $It_{max}$ is the number of iteration of this process. The process ends with $Ns_0 + Nr * \frac{Ns}{Nr} * It_{max}$ models. The used parameters are detailed in Tab. 6.

| $It_{max}$ | $Ns_0$ | $Ns$ | $Nr$ |
|---|---|---|---|
| 500 | 10000 | 100 | 100 |

Table 6: Tuning parameters of Neighborhood Algorithm.

During the inversion process, low velocity zones were not allowed. The Poisson ratio was inverted in each layer in the range 0.2-0.4 and the density was supposed equal to $2500\,\mathrm{kg/m^3}$ on the whole profile. Inversions with free layer depths as well as fixed layer depths were performed. 3 layers are enough to explain most of the targets (dispersion and ellipticity), but more layers are used to smooth the obtained results and better explore the parameter space. 5 independent runs of 5 different parametrization schemes (5 and 6 layers over a half space and 9, 10 and 11 layers with fixed depth) were performed. For further elaborations, the best models of these 25 runs were kept (Fig. 17).

The velocity profile is clearly layered. The $10$ first meters show a velocity of about $700\,\mathrm{m/s}$. At this depth, a clear interface is present with velocities below around $1500\,\mathrm{m/s}$ down to about $45\,\mathrm{m}$ depth. Below, hard rock is found and its velocity seems constrained around $2700\,\mathrm{m/s}$.

When compared to the target curves (Fig. 14), all Rayleigh modes are approximately reproduced. The picked curve from the transverse component of 3C array analysis as well as the H/V curve are displayed on Fig. 14 for comparison purposes. It shows that this curve is a mix of the fundamental and first higher mode. Ellipticity curve does not match perfectly but the trend is fine.

Another inversion has been conducted allowing for a velocity inversion in the upper part. It is then possible to perfectly reproduce the Rayleigh fundamental and second higher mode, the Love fundamental and first higher mode are also matching (Fig. 16). The first higher Rayleigh mode is not matching better, as well as the ellipticity. The inverted profiles are not very different from the previous ones (Fig. 17): the lower interface is located at $40\,\mathrm{m}$ depth, with velocity in the lower part of $2700\,\mathrm{m/s}$. Between $10$ and $40\,\mathrm{m}$ depth, the rock layer with a velocity of

$1400 - 1500\,\mathrm{m/s}$ is still present. In the upper part, a minimum velocity of $300\,\mathrm{m/s}$ (not very realistic) is found at $3\,\mathrm{m}$ depth. Higher velocities are found above and below. This peculiar behaviour may be very local and may not be relevant at SLUB site so that this inversion is not further used.

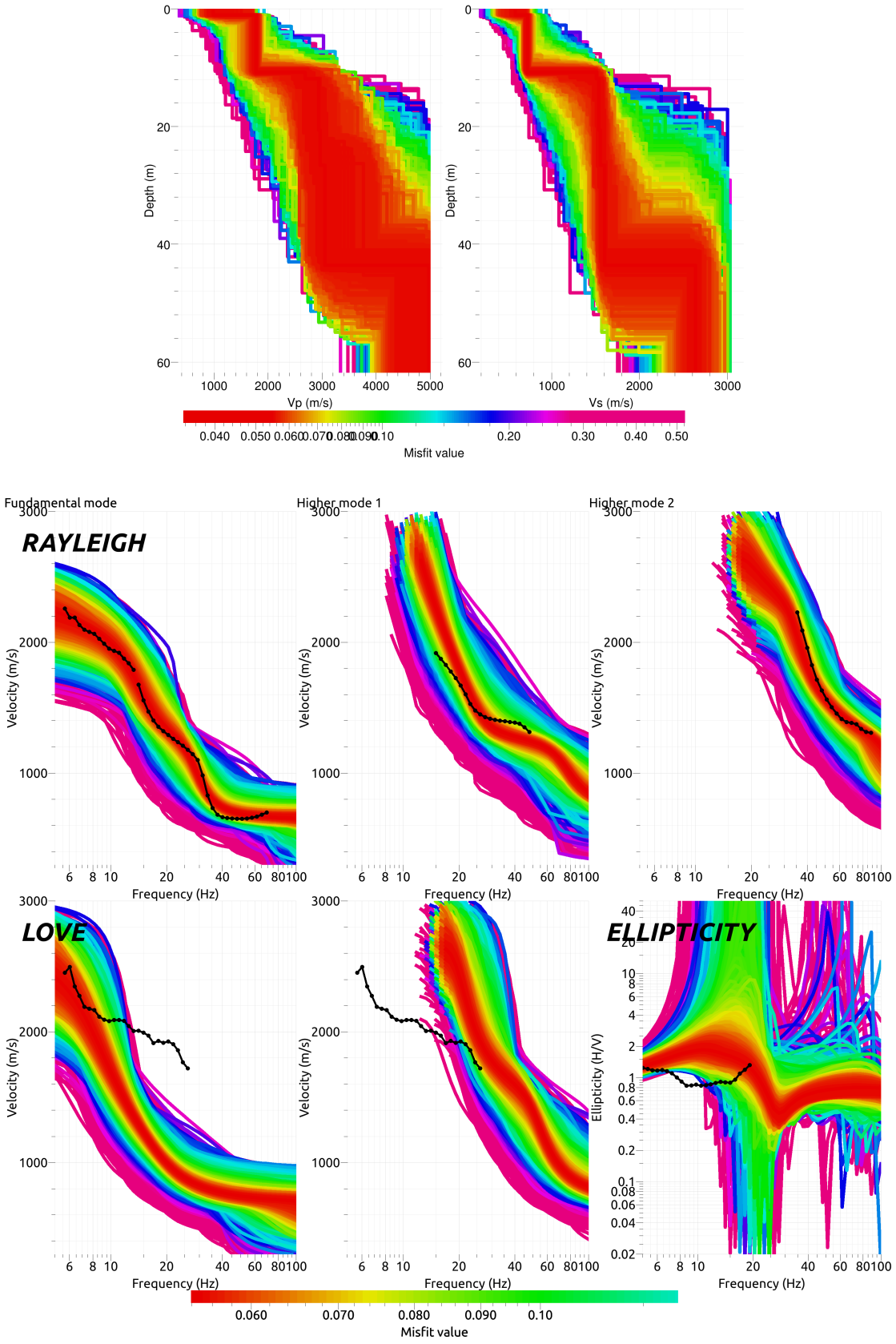


Figure 14: Top figure: Inverted ground profiles in terms of $V_p$ and $V_s$ (top); Bottom figure: comparison between inverted models and measured Rayleigh modes (top) and inverted Love modes (fundamental and first higher) compared to observed curve on the transverse component - not used - (bottom left and centre) and inverted ellipticity compared to the H/V curve - not used - (bottom right), free layer depth strategy.

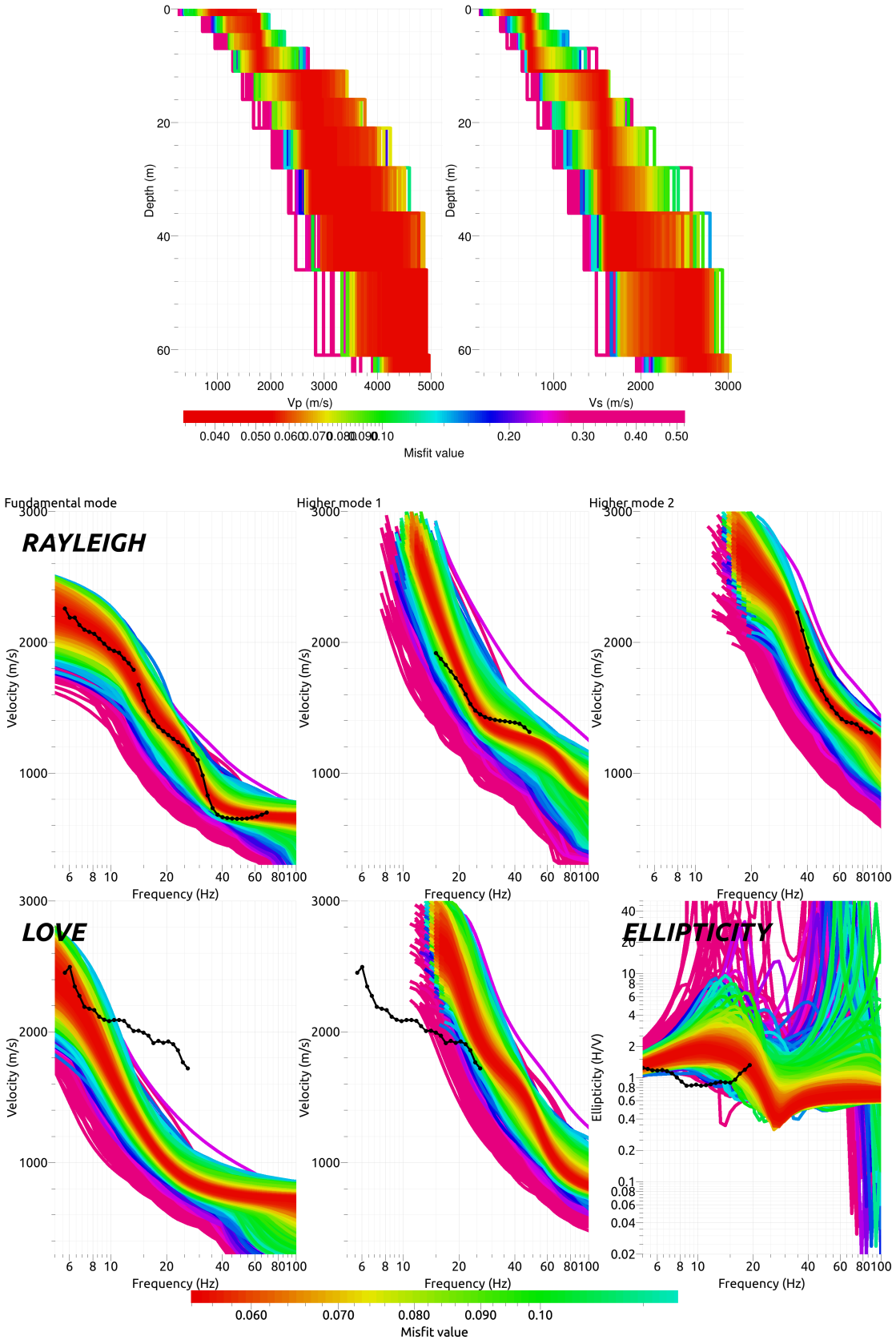


Figure 15: Top figure: Inverted ground profiles in terms of $V_p$ and $V_s$ (top); Bottom figure: comparison between inverted models and measured Rayleigh modes (top) and inverted Love modes (fundamental and first higher) compared to observed curve on the transverse component - not used - (bottom left and centre) and inverted ellipticity compared to the H/V curve - not used - (bottom right), fixed layer depth strategy.

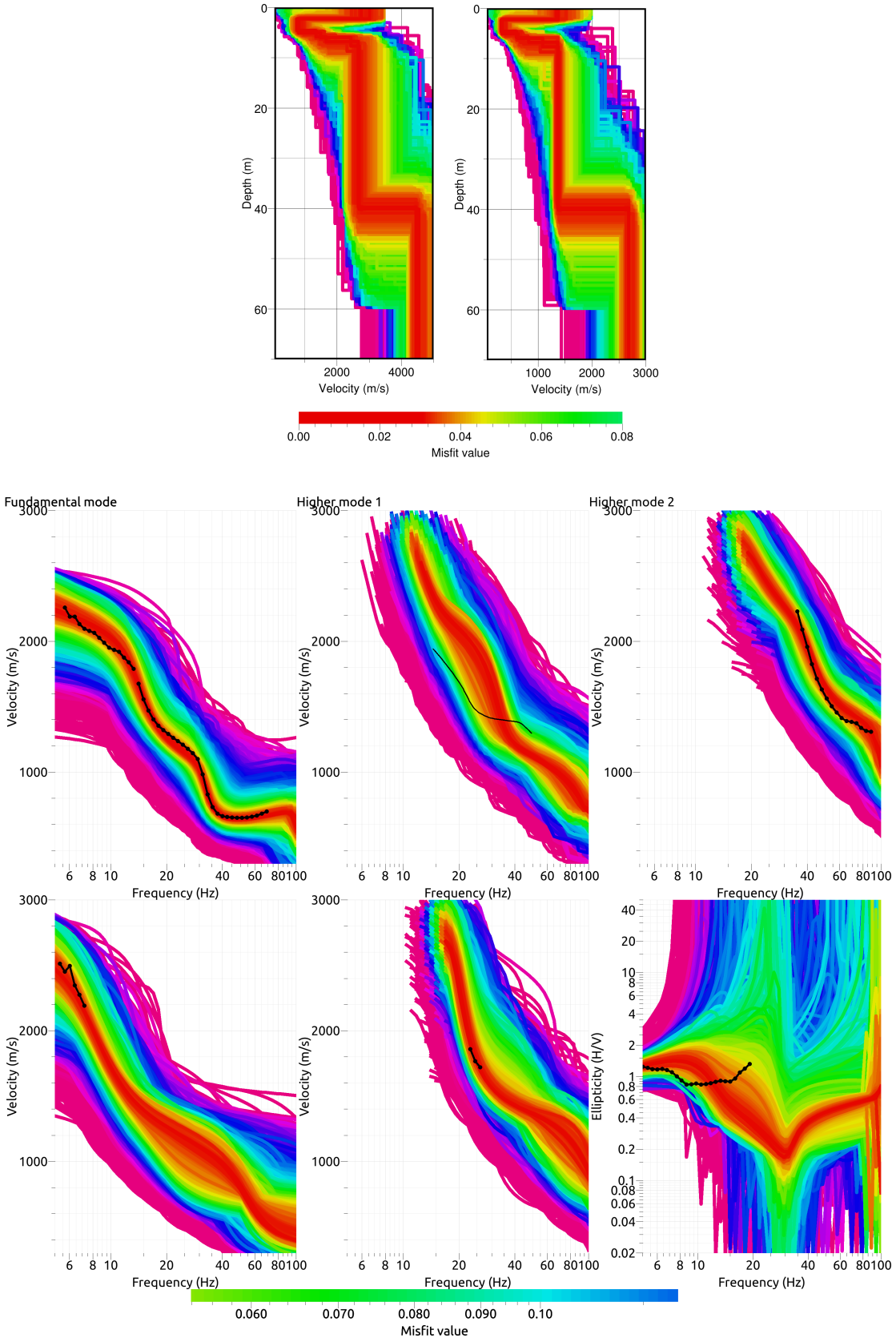


Figure 16: Same as Fig. 14 by allowing for a velocity inversion in the top part.

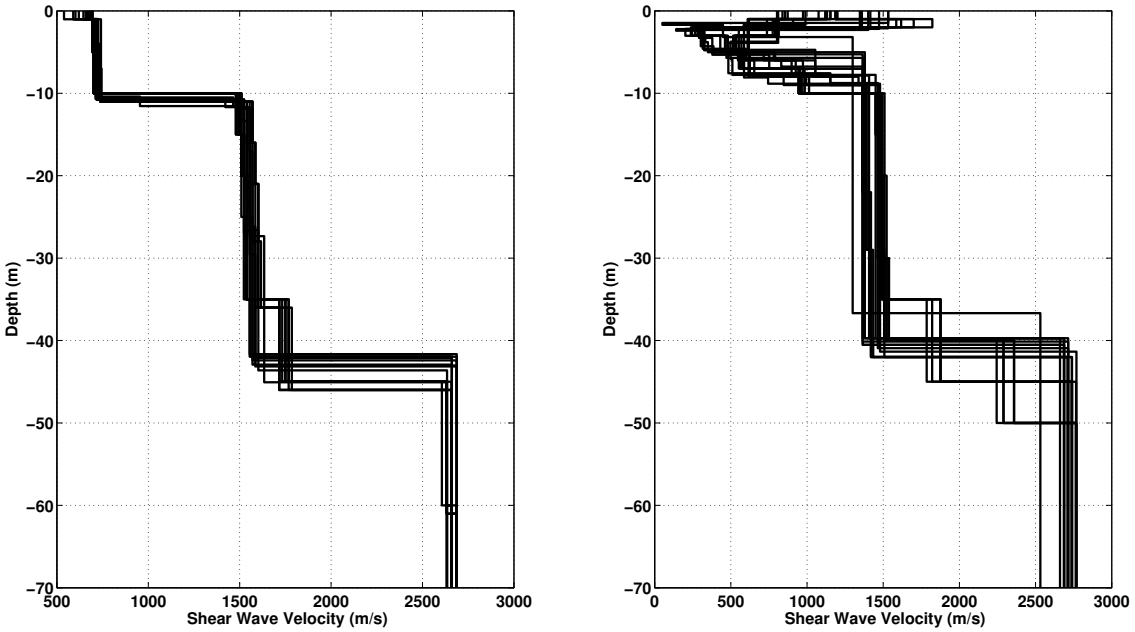


Figure 17: $V_s$ ground profiles for the 25 best models without velocity inversion (left), with velocity inversion (right).

## 6.2 Interpretation

A comparison with observed amplification at station SLUB obtained from earthquake recordings have been performed a posteriori [Edwards et al., 2013]. The first peak in the SH transfer function, related to the interface at $40 - 45\,\mathrm{m}$ depth, is found at $9\,\mathrm{Hz}$ for the obtained models (Fig. 17) but is located at higher frequency at SLUB ($13\,\mathrm{Hz}$), showing that this interface is located at a shallower depth. A quick computation leads to depths around $30\,\mathrm{m}$ at SLUB. It should be reminded that the active seismic experiment has been conducted $50\,\mathrm{m}$ away from SLUB, downhill, so that lateral variability is expected. The second layer may have been eroded more at the top of the hill than below. The second peak in the SH transfer function is shifted as well towards higher frequencies. SH transfer function of the set of profiles with the velocity inversion is not different from the one from the other profiles, showing again that the observed differences are due to lateral variability and not uncertainties in the inversion, even though the first $10\,\mathrm{m}$ are not clearly defined.

Therefore, 10 of the obtained profiles have been modified to shift the lower layer at about $30\,\mathrm{m}$ (Fig. 18). These models are selected for further computations. The amplitudes above $10\,\mathrm{Hz}$ are however not well reproduced in the 1D models (too large).

According to a rock outcrop and sampling when the station SLUB was installed, the first meters are made of a weak sandstone that can be crushed with the hand. Samples have been extracted to obtain the wave velocity of this sandstone.

## 6.3 Travel time average velocities and ground type

The distribution of the travel time average velocities at different depths was computed from the 10 selected models. The uncertainty, computed as the standard deviation of the distribution of travel time average velocities for the considered models, is also provided, but its meaning is doubtful since the parameter space was not fully explored. $V_{s,30}$ is found to be close to $1100\,\mathrm{m/s}$, that is associated to type A in the Eurocode 8 [CEN, 2004] and SIA261 [SIA, 2003].

| | **Mean (m/s)** | **Uncertainty (m/s)** |
|---|---|---|
| $V_{s,5}$ | 701 | 8 |
| $V_{s,10}$ | 711 | 4 |
| $V_{s,20}$ | 948 | 4 |
| $V_{s,30}$ | 1100 | 11 |
| $V_{s,40}$ | 1287 | 16 |
| $V_{s,50}$ | 1436 | 16 |
| $V_{s,100}$ | - | - |
| $V_{s,150}$ | - | - |
| $V_{s,200}$ | - | - |

Table 7: Travel time averages at different depths from the inverted models. Uncertainty is given as one standard deviation from the selected profiles.

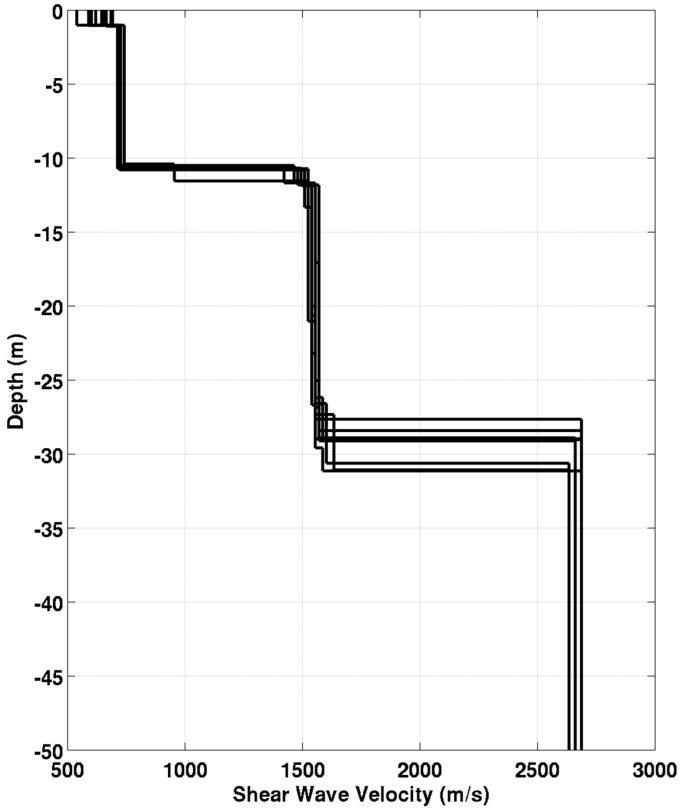


Figure 18: $V_s$ ground profiles for the 10 selected models for station SLUB.

## 6.4 Quarter-wavelength velocity and SH transfer function

The quarter-wavelength velocity approach [Joyner et al., 1981] provides, for a given frequency, the average velocity at a depth corresponding to 1/4 of the wavelength of interest. It is useful to identify the frequency limits of the experimental data (minimum frequency in dispersion curves at $5.6\,\mathrm{Hz}$ here). The results using this proxy show that the dispersion curves constrain the profiles down to $75\,\mathrm{m}$ (Fig. 19). Moreover, the quarter wavelength impedance-contrast introduced by Poggi et al. [2012b] is also displayed in the figure. It corresponds to the ratio between two quarter-wavelength average velocities, respectively from the top and the bottom part of the velocity profile, at a given frequency [Poggi et al., 2012b]. It shows a trough (inverse shows a peak) at the resonance frequency.
The theoretical SH-wave transfer function for vertical propagation [Roesset, 1970] is computed from the inverted profiles. It is compared to the quarter-wavelength amplification [Joyner et al., 1981], that however cannot take resonances into account (Fig. 20). In this case, the models are predicting an amplification above $10\,\mathrm{Hz}$ only.

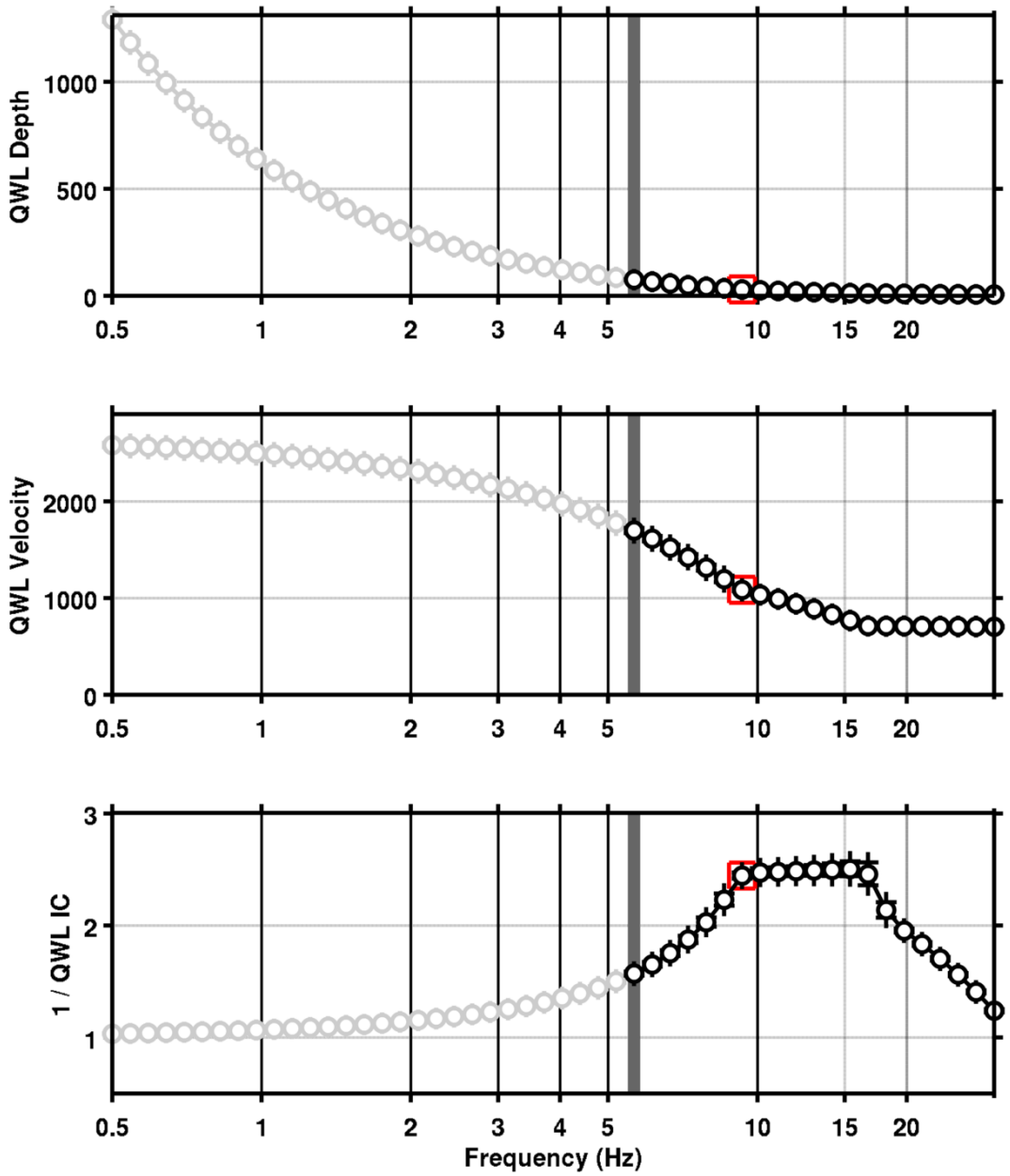


Figure 19: Quarter wavelength velocity representation of the velocity profile (top: depth, centre: velocity, bottom: inverse of the impedance contrast). Black curve is constrained by the dispersion curves, light grey is not constrained by the data. Red square is corresponding to $V_{s,30}$.

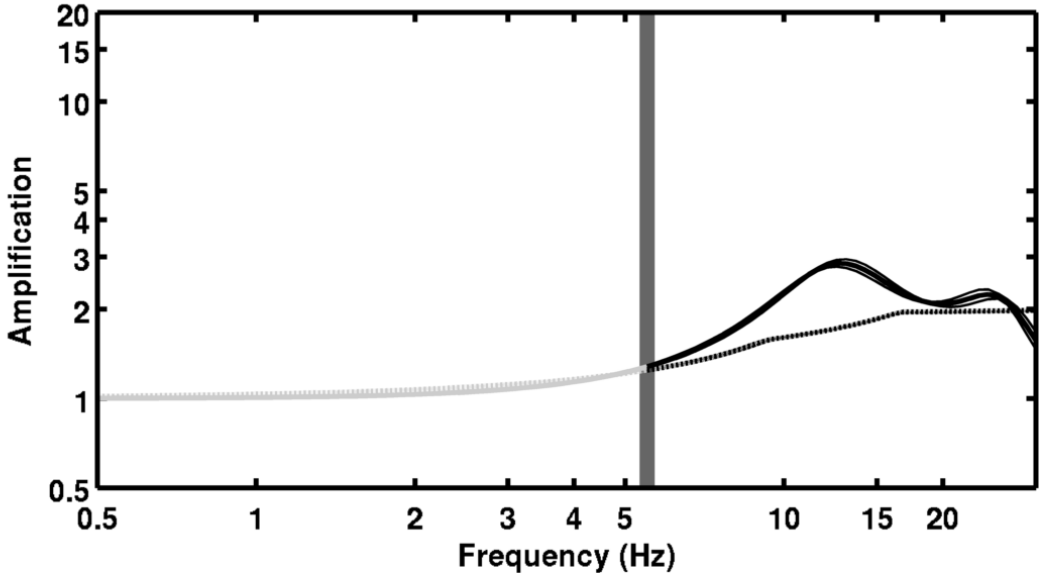


Figure 20: Theoretical SH transfer function (solid line) and quarter wavelength impedance contrast (dashed line) with their standard deviation. Significance of the greyshades is detailed in Fig. 19.

# 7 Conclusions

The combination of ambient vibration array measurements and active seismics presented in this study were successful in deriving a velocity model for the Bramberg site in Lucerne, below the SLUB station. The passive measurement allowed to constrain the deepest part of the profile down to $75\,\mathrm{m}$ according to the QWL proxy, whereas the active measurements could inform about the upper $15\,\mathrm{m}$. This combination was crucial in this case since a contrast was found at $10\,\mathrm{m}$ depth which could not have been seen only with passive measurements. The $10$ first meters show an unclear velocity profile, with possibly a velocity inversion. On average the velocity is about $700\,\mathrm{m/s}$ corresponding to a weathered sandstone, whereas the lower layer has velocities around $1500\,\mathrm{m/s}$ down to about $45\,\mathrm{m}$ depth at the tested site. However, at SLUB station, this interface is located around $30\,\mathrm{m}$ depth so that profiles were modified to reflect this. Below, hard rock is found with a velocity of about $2700\,\mathrm{m/s}$. $V_{s,30}$ is found to be close to $1100\,\mathrm{m/s}$ corresponding to EC8 and SIA261 ground types A.

# Acknowledgements

The authors thank Stefano Maranò and Lea Kiefer for the help during these measurements.

# References

Sylvette Bonnefoy-Claudet, Fabrice Cotton, and Pierre-Yves Bard. The nature of noise wavefield and its applications for site effects studies. *Earth-Science Reviews*, 79(3-4): 205–227, December 2006. ISSN 00128252. doi: 10.1016/j.earscirev.2006.07.004. URL http://linkinghub.elsevier.com/retrieve/pii/S0012825206001012.

J. Capon. High-Resolution Frequency-Wavenumber Spectrum Analysis. *Proceedings of the IEEE*, 57(8):1408–1418, 1969.

CEN. *Eurocode 8: Design of structures for earthquake resistance - Part 1: General rules, seismic actions and rules for buildings*. European Committee for Standardization, en 1998-1: edition, 2004.

Benjamin Edwards, Clotaire Michel, Valerio Poggi, and Donat Fäh. Determination of Site Amplification from Regional Seismicity: Application to the Swiss National Seismic Networks. *Seismological Research Letters*, 84(4):611–621, July 2013. ISSN 0895-0695. doi: 10.1785/0220120176. URL http://srl.geoscienceworld.org/cgi/doi/10.1785/0220120176.

Donat Fäh, Fortunat Kind, and Domenico Giardini. A theoretical investigation of average H / V ratios. *Geophysical Journal International*, 145:535–549, 2001.

Donat Fäh, Gabriela Stamm, and Hans-Balder Havenith. Analysis of three-component ambient vibration array measurements. *Geophysical Journal International*, 172(1):199–213, January 2008. ISSN 0956540X. doi: 10.1111/j.1365-246X.2007.03625.x. URL http://doi.wiley.com/10.1111/j.1365-246X.2007.03625.x.

Donat Fäh, Marc Wathelet, Miriam Kristekova, Hans-Balder Havenith, Brigitte Endrun, Gabriela Stamm, Valerio Poggi, Jan Burjanek, and Cécile Cornou. Using Ellipticity Information for Site Characterisation Using Ellipticity Information for Site Characterisation. Technical report, NERIES JRA4 Task B2, 2009.

William B. Joyner, Richard E. Warrick, and Thomas E. Fumal. The effect of Quaternary alluvium on strong ground motion in the Coyote Lake, California, earthquake of 1979. *Bulletin of the Seismological Society of America*, 71(4):1333–1349, 1981.

Katsuaki Konno and Tatsuo Ohmachi. Ground-Motion Characteristics Estimated from Spectral Ratio between Horizontal and Vertical Components of Microtremor. *Bulletin of the Seismological Society of America*, 88(1):228–241, 1998.

R.T. Lacoss, E. J. Kelly, and M. N. Toksöz. Estimation of Seimic Noise Structure using Arrays. *Geophysics*, 34(1):21–38, 1969.

V. Poggi, D. Fäh, and D. Giardini. Time,ÄìFrequency,ÄìWavenumber Analysis of Surface Waves Using the Continuous Wavelet Transform. *Pure and Applied Geophysics*, 170(3): 319–335, June 2012a. ISSN 0033-4553. doi: 10.1007/s00024-012-0505-5. URL http://www.springerlink.com/index/10.1007/s00024-012-0505-5http://link.springer.com/10.1007/s00024-012-0505-5.

Valerio Poggi and Donat Fäh. Estimating Rayleigh wave particle motion from three-component array analysis of ambient vibrations. *Geophysical Journal International*, 180(1):251–267, January 2010. ISSN 0956540X. doi: 10.1111/j.1365-246X.2009.04402.x. URL http://doi.wiley.com/10.1111/j.1365-246X.2009.04402.x.

Valerio Poggi, Benjamin Edwards, and D. Fah. Characterizing the Vertical-to-Horizontal Ratio of Ground Motion at Soft-Sediment Sites. *Bulletin of the Seismological Society of America*, 102(6):2741–2756, December 2012b. ISSN 0037-1106. doi: 10.1785/0120120039. URL http://www.bssaonline.org/cgi/doi/10.1785/0120120039.

Valerio Poggi, Donat Fäh, Jan Burjanek, and Domenico Giardini. The use of Rayleigh-wave ellipticity for site-specific hazard assessment and microzonation: application to the city of Lucerne, Switzerland. *Geophysical Journal International*, 188(3):1154–1172, March 2012c. ISSN 0956540X. doi: 10.1111/j.1365-246X.2011.05305.x. URL http://doi.wiley.com/10.1111/j.1365-246X.2011.05305.x.

J.M. Roesset. Fundamentals of soil amplification. In R. J. Hansen, editor, *Seismic Design for Nuclear Power Plants*, pages 183–244. M.I.T. Press, Cambridge, Mass., 1970. ISBN 978-0-262-08041-5. URL http://mitpress.mit.edu/catalog/item/default.asp?ttype=2\&tid=5998.

SIA. *SIA 261 Actions sur les structures porteuses*. Société suisse des ingénieurs et des architectes, Zürich, sia 261:20 edition, 2003.

Marc Wathelet. An improved neighborhood algorithm: Parameter conditions and dynamic scaling. *Geophysical Research Letters*, 35(9):1–5, May 2008. ISSN 0094-8276. doi: 10.1029/2008GL033256. URL http://www.agu.org/pubs/crossref/2008/2008GL033256.shtml.

# Appendix

This paragraph is describing the datasets of the active seismic experiment.

**Active dataset 1** Source type: weight drop, 1.13 m
Number of shots: 10 (files 1.dat to 10.dat)
Offset 18.5 m
Note:

**Active dataset 2** Source type: weight drop, 1.13 m
Number of shots: 10 (files 11.dat to 20.dat)
Offset 18.5 m
Note:

**Active dataset 3** Source type: weight drop, $1.13\,\mathrm{m}$
Number of shots: 10 (files 21.dat to 30.dat)
Offset $40\,\mathrm{m}$
Selection: [ all ]
Note:

**Active dataset 4** Source type: weight drop, $1.70\,\mathrm{m}$
Number of shots: 1 (file 31.dat)
Offset $40\,\mathrm{m}$
Note: with 1 damper under the weight

**Active dataset 5** Source type: weight drop, $1.70\,\mathrm{m}$
Number of shots: 3 (files 32.dat to 34.dat)
Offset $40\,\mathrm{m}$
Selection: [ all ]
Note: without damper under the weight

**Active dataset 6** Source type: weight drop, $1.13\,\mathrm{m}$
Number of shots: 6 (files 35.dat to 40.dat)
Offset $40\,\mathrm{m}$
Selection: [ all ]
Note: without damper under the weight